

pubs.acs.org/JPCC Article

Deciphering the Optical Absorption Spectra of Ultrafine Metal Nanoparticles Dispersed on Submicron Silica Spheres

Qilin Wei, Matas Simukaitis, Siyu Wu, Jonathan J. Foley, IV, and Yugang Sun*



ACCESS I III Metrics & More Article Recommendations Supporting Information Pt nanoparticles Resonant **Photonic** Diffusive scattering reflection scattering of silica spheres Break-down of Pt absorption Silica spheres 750 450 300 Wavelength (nm)

ABSTRACT: Optical absorption of metal nanoparticles on dielectric supports that do not absorb light becomes complicated due to the convolution of light scattering of the dielectric supports. Identifying the origin of optical absorption characteristics in metal/dielectric composite materials is vital to designing materials with desirable optical absorption properties for interesting applications such as photocatalysis. In this work, we systematically investigated the optical absorption of ultrafine metal nanoparticles (ufMNPs) supported on silica spheres (SiO_x-SPs) using absorption-sensitive diffuse reflectance spectroscopy (DRS) and theoretical modeling/calculations. The comparisons between experimental measurements and theoretical predictions reveal that the SiO_x-SPs in ufMNPs/SiO_x-SP composite powders exhibit three types of scattering to determine the optical absorption of the supported ufMNPs. First, localized light-scattering resonances near the surface of individual SiO_x-SPs with large sizes generate enhanced electric fields to promote strong optical absorption in the ufMNPs with well-defined peaks. Second, nonunidirectional diffuse light scattered from individual SiO_x-SPs with relatively small sizes penetrates the composite powders to be absorbed by the ufMNPs, exhibiting uphill and peakless absorption profiles. Third, the diffuse light can be modulated by the ordered packing of the composite particles that exhibit photonic reflection at the stop band, resulting in a valley in the DRS spectrum of a composite powder. The deconvolution of optical absorption in the ufMNPs/SiO_x-SP composite particles opens an avenue to rationally design composite materials with favorable light absorption properties, for example, nonlinearity of localized absorption versus linearity of diffuse absorption.

1. INTRODUCTION

Light absorption in metal nanoparticles originating from surface plasmon resonances has been extensively studied for photoenergy conversion, including photothermal effect 1-6 and hot-carrier chemistry. 7-11 The conversion efficiency of the photoenergy absorbed in metal nanoparticles usually increases with the decrease of the size of the nanoparticles below 10 nm due to surface damping and/or chemical interface damping. 12-14 However, size reduction significantly weakens light absorption power in individual metal nanoparticles, in particular, metal nanoparticles lacking surface plasmon resonances in the visible spectral region. The weak light absorption power prevents efficient harvesting of the incident light, deteriorating the overall energy conversion efficiency of the incident light. Light antennae can spatially concentrate the energy of incident light to increase the photoenergy absorbed in individual small metal nanoparticles even when the incident

light is constant. Integrating small metal nanoparticles with appropriate light antennae represents a powerful strategy to amplify light absorption power in individual metal nanoparticles. For example, plasmonic nanostructures which exhibit enhanced electric fields near their surfaces in light have been evaluated as light antennae to improve light absorption in small metal nanoparticles that are carefully placed near the plasmonic nanostructures with desirable dielectric spacings. 15–19 Controlling the composition and thickness of the

Received: June 21, 2022 Revised: September 30, 2022 Published: October 18, 2022





dielectric spacers is not trivial because the electric fields decay exponentially with the distance from the plasmonic antenna surface. When the dielectric spacers are too thick, the enhancement of electric fields becomes too weak to support strong light absorption in the small metal nanoparticles.² Thin dielectric spacers may cause an electric crossover (i.e., charge transfer) between the plasmonic antennae and the small metal nanoparticles, changing the properties of the metal nanoparticles. The plasmonic antennae absorb light to support the enhanced local electric fields, but the absorbed light eventually decays to heat in the antennae and cannot be absorbed by the small metal nanoparticles. On the other hand, dielectric structures with appropriate geometries can also generate enhanced electric fields near their surfaces due to Fabry-Perot or Whispering Gallery resonances (Figure S1), making them suitable for a class of light antennae. ^{22–25} Because of the insulation nature of dielectric antennae, small metal nanoparticles can be directly loaded onto the surfaces of the antennae to benefit from the enhanced electric fields. We have synthesized composite materials made of ultrafine metal nanoparticles (with a size of <10 nm) dispersed on submicron silica spheres (with sizes of 200-450 nm). 26-29 The presence of the ultrafine metal nanoparticles does not diminish the strong surface scattering resonances on the silica spheres (Figure S2), resulting in the observation of significantly enhanced light absorption in the metal nanoparticles (Figure $S3).^{26}$

The promise of submicron silica spheres as light antennae to enhance light absorption in small metal nanoparticles has motivated us to explore metal/silica composites in photocatalysis.^{27,28,30,31} The light scattering resonances near the surface of silica spheres (SiO_x-SPs) under light irradiation depend on their sizes. The size-dependent resonant spectra can directly translate to enhanced light absorption in ultrafine metal nanoparticles (ufMNPs) loaded on SiO_x-SPs. The light scattering resonances represent localized phenomena near the surface of individual SiO_x-SPs, and the correspondingly enhanced optical absorption in the ufMNPs is independent of the number and packing condition of the ufMNPs/SiO_x-SP composite particles. On the other hand, the light scattering by the submicron SiO_x-SPs influences light propagation in powder samples of packed ufMNPs/SiO_x-SP composite particles (e.g., fixed-bed catalysts), affecting light absorption in the buried particles. Herein, we systematically study the optical absorption of ufMNPs/SiO_x-SP composite powders at varying packing densities to distinguish the contributions of localized light scattering resonances near the SiO_x-SP's surfaces and the diffuse light penetrated the packed powder ensembles. The former contribution locally intensifies the electric fields near the SiO_x-SP's surfaces compared to the electric field of the incident light, enhancing light absorption in ufMNPs with characteristic peaks determined by the scattering resonance bands of SiO_x-SPs. This portion is referred to as localized absorption (with enhancement). The latter light contribution with random propagation directions diffuses in the powder samples to be absorbed in the supported ufMNPs without localized enhancement. This portion is referred to as (globalized) diffuse absorption.

2. EXPERIMENTAL SECTION

2.1. Synthesis of Ultrafine Pt Nanoparticles. Pt nanoparticles were synthesized to evaluate their optical absorption upon being loaded on SiO_x -SPs because the

freestanding Pt nanoparticles with ultrafine sizes exhibited only broadband and peakless absorption spectra. At room temperature, 26 mL of aqueous solution of 2.8 mM sodium citrate (Alfa Aesar) was added to 50 mL of aqueous solution of 0.4 mM hexachloroplatinic(IV) acid (Sigma–Aldrich) under vigorous stirring. After 1 min, to this solution was added 5 mL of freshly prepared 12 mM sodium boron hydride (Alfa Aesar) aqueous solution dropwise at a rate of 1 mL min⁻¹. The solution became dark brown in 5 min and continued aging for 2 h. The resulting colloidal Pt ufMNPs were stored and used without further purification.

2.2. Synthesis and Surface Functionalization of SiO_x-**SPs.** Monodisperse SiO_x-SPs were synthesized through a modified Stöber method based on controlled hydrolysis of tetraethyl orthosilicate (TEOS, Sigma-Aldrich). In a typical synthesis of SiO_x-SPs with an average diameter of 353 nm, 10.88 mL of TEOS was added to a solution containing 120 mL of isopropyl alcohol (Fisher Scientific), 45.60 mL of deionized water, and 24.60 mL of ammonia hydroxide (28-30 wt % in water, Fisher Scientific) under magnetic stirring at 40 $^{\circ}\text{C}.$ The solution turned to milky-white in 1 min due to the hydrolysis of TEOS and condensation of hydrolysates into silica nanoparticles. The hydrolysis reaction continued for 2 h, completing the growth of SiO_x-SPs. The resulting SiO_x-SPs were collected from centrifugation and washed with ethanol, which was repeated two times. The collected SiO_x-SPs were then dried overnight in an oven at 60 °C. SiO_x-SPs with different diameters ranging from 100 to 1100 nm were synthesized by slightly adjusting the reaction conditions, including the volume of solvent, the volume of TEOS, and temperature. The reaction conditions and the average diameters of the synthesized SiO_x-SPs are summarized in Table S1 (Supporting Information). The as-synthesized SiO_x-SPs exhibited negatively charged surfaces. Surface modification with (3-aminopropyl) triethoxysilane (APTES, Acros Organics) was performed to change their surfaces to be positively charged. In a typical modification process, 400 mg of dried SiO_x-SPs was dispersed in 200 mL of ethanol (190 proof, Pharmco-Aaper) with the assistance of ultrasonication. To this dispersion was added dropwise 2 mL of APTES at 60 °C. The reaction continuously proceeded for 8 h to conjugate APTES to the surface of the SiO_x-SPs. The powders were washed with ethanol twice and collected via centrifugation. The APTES-modified SiO_x-SPs were dried in an oven at 60 °C

2.3. Loading of Pt ufMNPs onto SiO_x-SPs. In a typical process of loading 2 wt % Pt ufMNPs onto SiO_x-SPs, 41.52 mL of dispersion of the Pt ufMNPs synthesized in Section 2.1 was slowly added to 100 mL of aqueous dispersion containing 100 mg of APTES-functionalized SiO_x-SPs under vigorous stirring. The mixture was continuously stirred for 1 h to fully load the Pt ufMNPs to the SiO_x surface through electrostatic attraction. The resulting ufMNPs/SiO_x-SP composite particles were collected through centrifugation. The collected composite particles were washed with water/ethanol 2 times, followed by drying at 60 °C in an oven. The colorless and transparent supernatant indicated that the ufMNPs were completely attached onto the surface of SiO_x-SPs.

2.4. Characterization. Scanning electron microscopy (SEM) images were recorded with a microscope (FEI Quanta FEG 450) operated at a high-vacuum mode with an acceleration voltage of 10 kV. A transmission electron microscope (TEM, JEOL JEM—1400) was used to image the

synthesized samples. The diffuse reflectance spectroscopy (DRS) study was performed with a commercial ultraviolet—visible (UV—vis) spectrophotometer (Thermo Scientific, Evolution 220) equipped with an integrating sphere. The light source in the spectrophotometer is a built-in xenon flash lamp. The setup configuration of sample placement is highlighted in Figure S4. The extinction spectra were measured with the traditional transmission mode by placing samples between the light source and the traditional photodetector.

3. RESULTS AND DISCUSSION

Optical absorption of powder samples can be characterized by DRS that can exclude the size-dependent scattering to provide accurate light absorption in samples containing light-absorbing constituents. DRS becomes suitable for evaluating the light absorption of ufMNPs loaded on SiO_x -SPs of different sizes that do not absorb light but exhibit different scattering behaviors. Highly uniform SiO_x -SPs with different diameters (112–1089 nm) have been synthesized (Figure S5), and Pt ufMNPs have been attached to the surfaces of the SiO_x -SPs at controlled loadings (i.e., 1.0 and 2.5 wt %) (Figure S6). The narrow size distributions (i.e., <5% except for the 112 nm sample) of the SiO_x -SPs confirm that the differences in optical absorption spectra of the ufMNPs/SiO $_x$ -SP composite particles originate from the size difference of the SiO_x -SPs rather than size distributions. Figure 1a presents the Pt ufMNPs

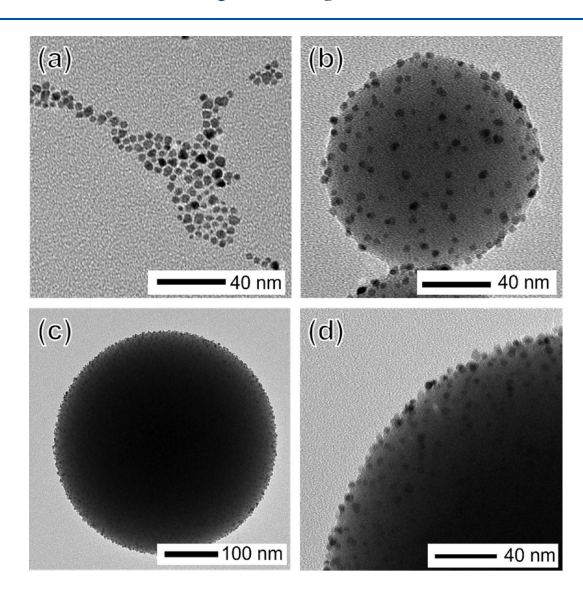


Figure 1. TEM images of (a) freestanding Pt ufMNPs with an average diameter of 3.9 (± 0.6) nm and (b, c) individual Pt-ufMNPs/SiO_x-SP composite particles composed of 2.5 wt % Pt ufMNPs on SiO_x-SPs with diameters of (b) 112 and (c) 441 nm. (d) Blowup image of a partial composite particle shown in (c), highlighting the good dispersion of Pt ufMNPs on the SiO_x-SP surface and the absence of agglomeration of the Pt ufMNPs.

synthesized through the reduction of hexachloroplatinic acid in the presence of citrate that stabilizes the Pt ufMNPs with negatively charged surfaces. The Pt ufMNPs exhibit an average size of 3.9 nm and a standard deviation of 0.6 nm, and their aqueous dispersion exhibits weak broadband absorption without characteristic peaks in the visible spectral region (Figure S7a). The powder SiO_x-SPs exhibit almost no optical absorption in the UV–vis spectral region regardless of the surface modification (Figure S7b). The SiO_x-SPs modified

with APTES exhibit positively charged surfaces, which attract the negatively charged Pt ufMNPs coated with citrate through electrostatic attractions upon mixing. The spontaneous self-assembly results in uniform dispersion of Pt ufMNPs on the SiO_x -SPs (Figure 1b-d). The high dispersion of the Pt ufMNPs on the SiO_x surfaces excludes the possible influence of interparticle coupling on the optical absorption in the supported Pt ufMNPs. The difference in optical absorption between the Pt-ufMNPs/SiO_x-SP composite particles and freestanding Pt ufMNPs is therefore ascribed to the unique scattering properties of packed SiO_x -SPs.

Rayleigh scattering dominates the scattering of particles with sizes below ~100 nm, exhibiting peakless spectra with an inverse proportionality of light wavelength (λ) to the 4th power (i.e., $\propto \lambda^{-4}$) and proportionality of the particle size to the 6th power.³² The monotonic decrease of Rayleigh scattering intensity as a function of light wavelength can be translated to a monotonic increase of diffuse light in the packed particle powders, resulting in an uphill spectral curve in the visible region. Figure 2a presents the DRS spectrum of the Pt ufMNPs supported on mesoporous silica nanoparticles with irregular morphologies and sizes smaller than 40 nm (Figure S6b), showing the increase of absorbance with wavelength. The absence of peaks and high absorbance make the powder to have a dark gray appearance (inset, Figure 2a). Weak Rayleigh scattering of small silica nanoparticles allows a large portion of incident light to penetrate the powder samples, resulting in a large number of Pt ufMNPs interacting with the penetrated light to absorb the optical energy. Increasing the size of silica particles intensifies Rayleigh scattering, lowering the percentage of incident light penetrating the powder samples. For example, when SiO_x-SPs are larger than 100 nm, the dominating scattering will transit from the peakless Rayleigh scattering to Mie scattering with the increased particle size in the studied spectral range. Since Mie scattering is not strongly wavelength dependent, the corresponding absorption of the Pt ufMNPs supported on the SiO_x-SPs exhibits weak wavelength dependence for large SiO_x-SPs (Figure 2b,c). The broadband uphill absorption exists for the SiO_x-SPs with sizes up to 353 nm (Figure 2b), and the uphill profile disappears for the larger SiO_x -SPs (Figure 2c). It is worth pointing out that absorption peaks can be observed in these samples except for the SiO_x-SPs with a size of 112 nm. The number of absorption peaks increases with the size of the SiOx-SPs. The direct incident light interacts with the top layers of SiO_x-SPs to generate strong surface scattering resonances (portion I, Figure 2d) because of the highly symmetric geometry of the SiO_x-SPs and the coherent phase of the direct incident light near the individual SiOx-SPs, resulting in enhanced electric fields at resonant wavelengths near the surfaces of individual top-layer SiO_x-SPs. It is worth pointing out that the total output of the xenon lamp is not entirely coherent in phase. However, the incident light near an individual SiO_x-SP could be considered to exhibit the same phase because its size is comparable to the light wavelength and much smaller than the xenon lamp. The SiO_x-SPs behave as light antennae to concentrate the incident light at specific resonant bands and thus enhance optical absorption in the supported Pt ufMNPs. Therefore, the Pt ufMNPs attached to the surface of the top layers of SiO_x-SPs exhibit optical absorption with peaks consistent with the scattering resonance bands.²⁶ These absorption peaks are localized absorption with enhancement. The light scattered off the incident direction behaves differently from the direct

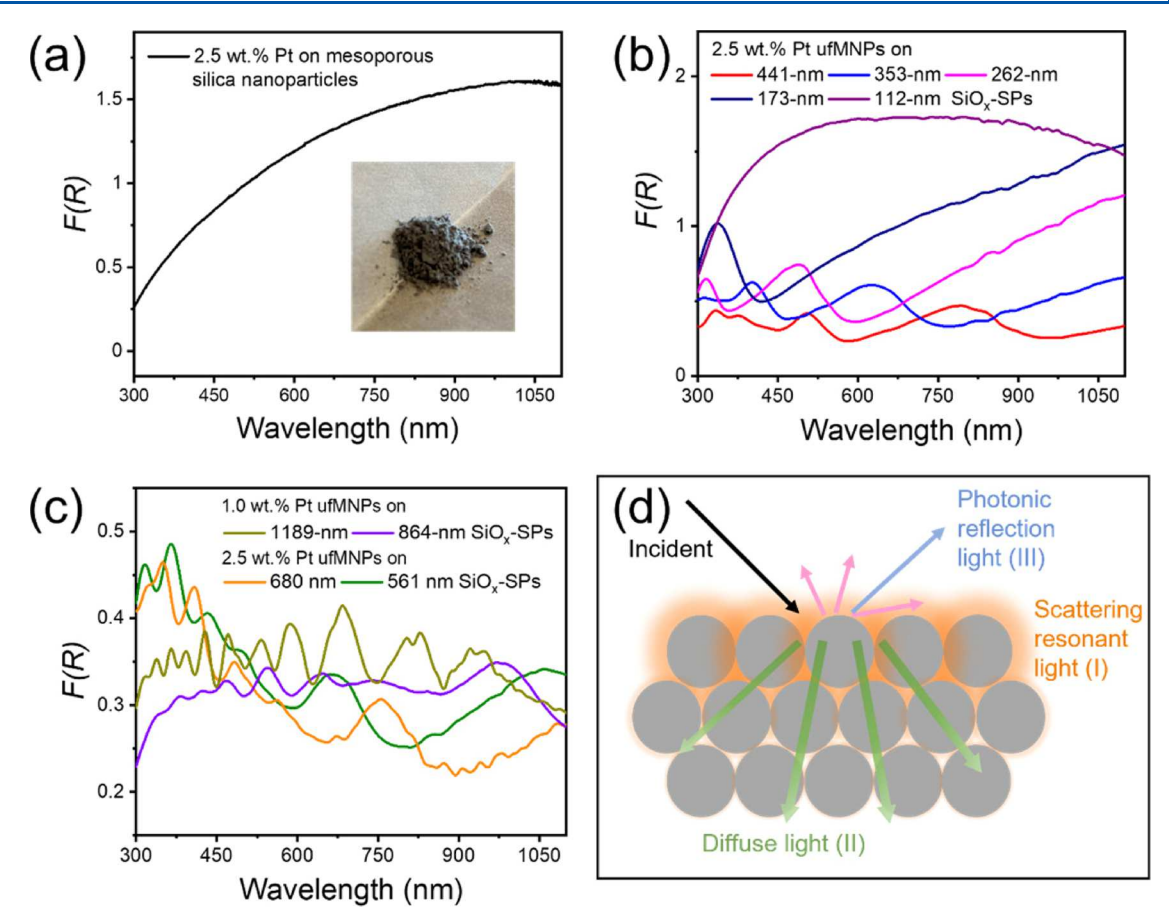


Figure 2. (a) DRS spectrum of the powder composed of 2.5 wt % Pt ufMNPs on mesoporous silica nanoparticles with irregular morphologies. The inset shows a photo of the powder showing a dark gray color. (b, c) DRS spectra of the Pt-ufMNPs/SiO_x-SP composite powders containing SiO_x-SPs with different sizes ranging from 112 to 1089 nm. The Pt ufMNP loading was 2.5 wt % for the powders containing SiO_x-SPs with sizes from 112 to 680 nm. The powders containing 864 and 1089 nm SiO_x-SPs had 1.0 wt % loading of Pt ufMNPs because of the lower mass-specific surface area of the large SiO_x-SPs. (d) Schematic diagram highlighting various optical scattering processes in Pt-ufMNPs/SiO_x-SP composite particles under light illumination. Due to the surface roughness of the powder, diffuse reflectance (pink arrows) happens on the powder surfaces and has minor interaction with the composite particles. Scattered lights into the powder are divided into three portions. Strong localized surface scattering resonances (portion I) occur near the surfaces of individual SiO_x-SPs in the few top layers of composite particles, which is indicated by the glowing orange color. The strength of localized surface scattering resonance decreases for the buried particles, which is indicated by the diluted glowing intensity. The green arrows indicate the diffuse light (portion II) penetrating the powder due to forward Mie scattering of SiO_x-SPs. The diffuse light can reach the buried particles to be absorbed in the Pt ufMNPs. The photonic reflection of light of specific wavelengths (portion III) happens due to the self-assembly of uniform-sized SiO_x-SPs into ordered superlattices (or photonic crystals). The presence of portion III indicated by the light blue arrows weakens portion II.

incident light to interact with the Pt-ufMNPs/ SiO_x -SP composite particles, showing the diffuse absorption with uphill profiles.

According to Mie theory, 33 extinction spectra of the freestanding single Pt nanoparticle and SiO_x-SPs of different sizes can be calculated (Figure S8). The optical extinction of Pt ufMNPs with a size of 4.0 nm originates only from absorption, while the extinction of SiO_x-SPs is solely ascribed to scattering in the UV-vis-NIR spectral region (300-1100 nm) that we have experimentally studied. The absorption spectrum of a Pt ufMNP exhibits a downhill-tailed profile without any characteristic peaks (dashed curve, Figure S8a). The scattering spectra of small SiO_x-SPs (e.g., 112 and 173 nm in diameter) exhibit similar long-tail profiles without apparent peaks, indicating the lack of scattering resonances near the surfaces of small SiO_x-SPs. When the SiO_x-SPs are large enough (e.g., 262 nm in diameter), localized light scattering resonances become strong enough to exhibit apparent scattering peaks. The scattering resonance peak for the 262 nm SiO_x-SP is

embedded in the predominant diffuse profile and displays as a shoulder peak at ~400 nm (green curve, Figure S8a). Further increasing the size of the SiO_x-SPs increases the strength of scattering resonances and the number of resonance peaks, which agrees with the measured scattering spectra of the SiO_x-SP powders (Figure S9). Comparing the theoretically calculated scattering spectra of the SiO_x-SPs with the measured absorption spectra of Pt-ufMNPs/SiO_x-SP composite particles reveals two aspects: (i) the absorption peaks of the composite particles with large SiO_x-SPs agree well with the theoretically calculated scattering spectra of the corresponding SiO_x-SPs (Figure 2c versus Figures S10, S8, and Table S2), highlighting that the localized scattering resonances near individual SiO_x-SPs of large sizes dominate the light absorption in the supported Pt ufMNPs; and (ii) an additional strong and broad absorption peak at longer wavelength is observed for each composite sample with SiO_x-SPs of 561 nm in diameter and smaller ones compared to the calculated scattering spectra of the corresponding SiO_x-SPs (Figure 2b versus Figures S10a

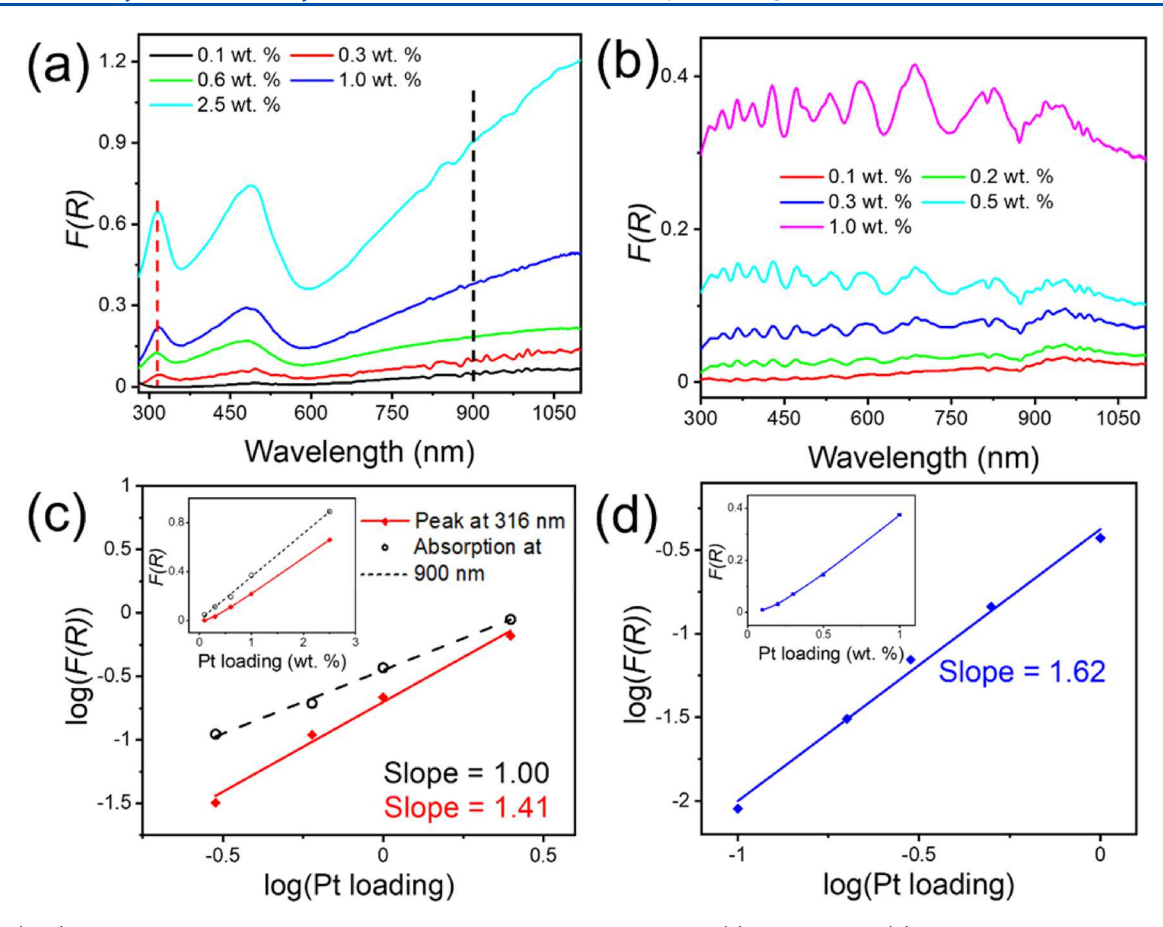


Figure 3. (a, b) DRS spectra of Pt-ufMNP/SiO_x-SP composite powders containing (a) 262 nm and (b) 1089 nm SiO_x-SPs and different Pt loadings. (c, d) DRS intensity as a function of Pt loading for (c) peak at 312 nm and an uphill point at 900 nm presented in (a), and (d) average of all peaks presented in (b). The dependences are plotted in the log-log function, and the insets represent the normal-normal plots. The linear log-log plots show a linear dependence of DRS intensity on Pt loading (slope = 1) or superlinear dependence (slope > 1).

and S8, and Table S2), indicating that the diffuse absorption in the supported Pt ufMNPs is influenced by the packing of ensembled Pt-ufMNPs/SiO $_x$ -SP composite particles.

Light scattering by the top layers of SiO_x-SPs attenuates the light that can diffuse into the Pt-ufMNPs/SiO_x-SP composite powders. The diffuse light (portion II, Figure 2d) lacks phase coherence near the surface of individual SiO_x-SPs due to the nonunidirectional feature of light scattering. The diffuse light weakens surface scattering resonances near the buried SiO_x-SPs in the composite powders. Therefore, the diffuse light is expected to give peakless absorption spectra with uphill tails in the supported Pt ufMNPs similar to the absorption spectrum of the Pt ufMNPs supported on mesopore silica nanoparticles shown in Figure 2a. The contribution of diffuse light to the absorption in the supported Pt ufMNPs decreases with the size of SiO_x-SPs. In addition, the high size uniformity of the SiO_x-SPs favors the Pt-ufMNPs/SiO_x-SP composite particles to selfassemble into ordered superlattices (or photonic crystals, Figure S11), which exhibit size-dependent characteristic stop bands in the reflection spectra (portion III, Figure 2a). The photonic reflection of a sample reduces the overall intensity of diffuse light, and the photonic reflection peak determined by the stop band is translated to a valley in the spectrum of diffuse light and the absorption spectrum of the corresponding PtufMNPs/SiO_x-SP composite powder. The valley in an uphilltailed absorption spectrum creates a peak right before the valley. Therefore, the broad peak at the long wavelength in the DRS spectrum of a Pt-ufMNPs/SiO_x-SP composite sample is

ascribed to the photonic effect. For example, the photonic crystal formed from the Pt-ufMNPs/SiO_x-SP composite particles containing 262 nm SiO_x-SPs is predicted to exhibit the first-order reflection peak at 578 nm by using the averaged medium model (Figure S12). The details of modeling and calculations are described in Supporting Information (Procedure 3). The DRS spectrum of the corresponding composite powder shows a broad peak at 488 nm accompanied by a valley at 585 nm, which agrees well with the predicted position (578 nm) of the photonic reflection peak. A similar broader peak is also observed in the DRS spectrum of composite powder containing SiO_x-SPs with a diameter of up to 441 nm. The peak position shifts to red as the size of SiO_x-SPs increases because the photonic reflection peak redshifts with the size of SiO_x-SPs. The valley positions of the DRS spectra also agree well with the calculated peak positions of first-order photonic reflection (Table S3 and Figure S13). The absorption peak originated from the diffuse light with attenuation of photonic effect is asymmetric with a fronting profile. Careful comparison of the calculated scattering resonance peaks and the measured DRS peaks reveals that the absorption of the supported Pt ufMNPs originating from the first-order scattering resonance peak of the SiO_x-SPs (green numbers in Table S2) is embedded in the left side of the asymmetric peak with a fronting profile.

In the studied spectral region of 300–1100 nm, optical absorption in Pt-ufMNPs/SiO $_x$ -SP composite powders originates from absorption by the Pt ufMNPs but is significantly

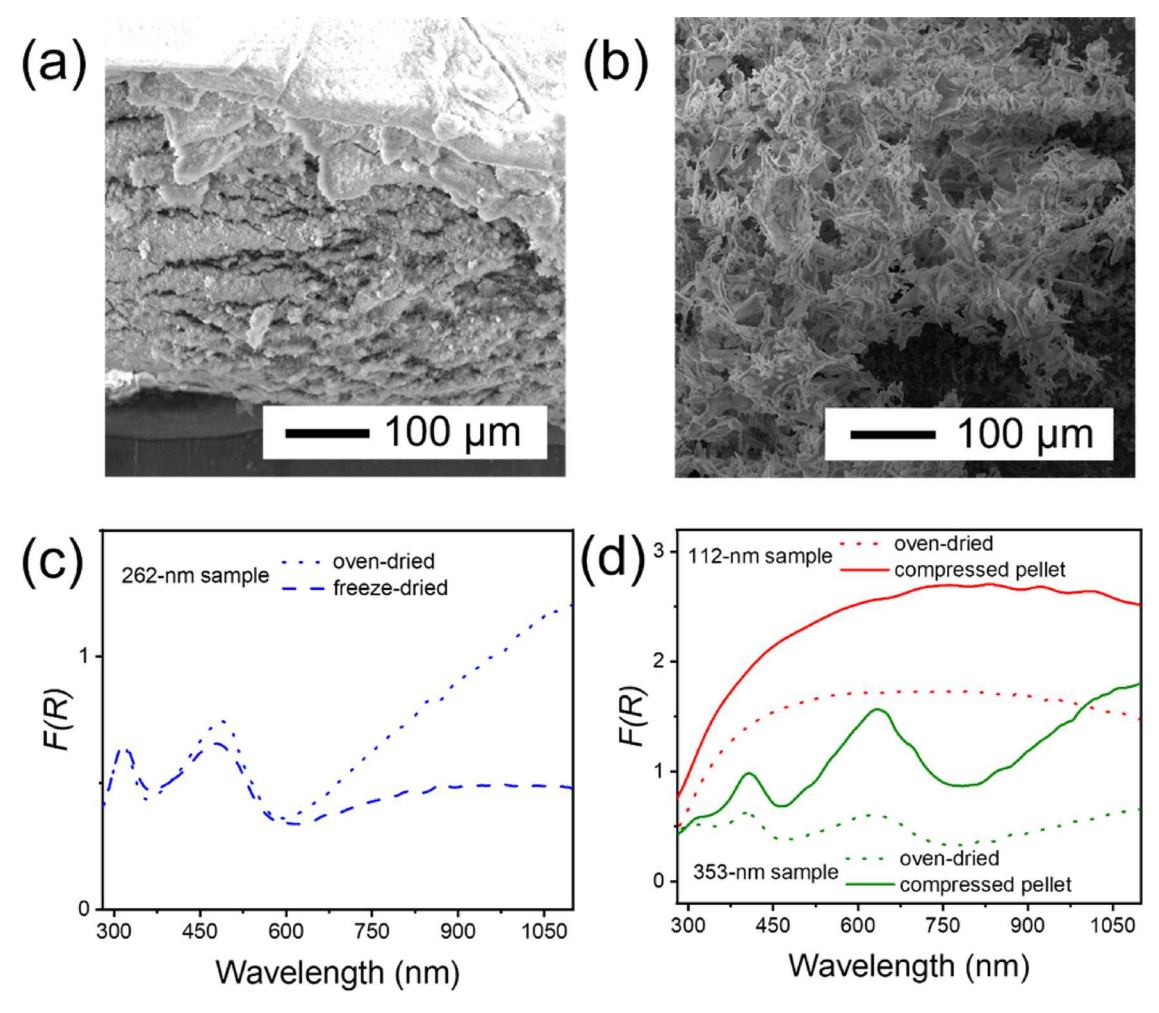


Figure 4. SEM images of (a) oven-dried and (b) freeze-dried Pt-ufMNPs/SiO_x-SP composite particles composed of 2.5 wt % Pt ufMNPs and 262 nm SiO_x-SPs. (c) DRS spectra of the composite particles presented in (a) and (b), displayed by the dotted and dashed curves, respectively. (d) DRS spectra of oven-dried powders (dotted curves) and pressed pellets (solid curves) of Pt-ufMNPs/SiO_x-SP composite particles composed of 2.5 wt % Pt ufMNPs on 112 nm (red curves) and 353 nm (green curves) SiO_x-SPs.

modulated by the scattering of SiO_x -SPs. The scattered light by the SiO_x-SPs is classified into two categories: localized scattering resonances near the surface of individual SiO_x-SPs (portion I, Figure 2d) and diffuse light into the composite powders (portion II, Figure 2d) attenuated by photonic reflections (portion III, Figure 2d). The localized surface scattering resonances mainly occur near the SiO_x-SPs of the few top layers that can interact with the direct incident light or slightly tuned incident light, resulting in enhanced optical absorption in the supported Pt ufMNPs with the appearance of narrow peaks determined by the scattering resonance bands. The contribution of localized absorption increases with the size of SiO_x-SPs. The attenuated diffuse light leads to optical absorption with an uphill-tailed profile and a broad asymmetric peak overlapping a localized absorption peak on the fronting side. The contribution of diffuse light to optical absorption becomes weak as the size of SiO_x-SPs increases. The PtufMNPs/SiO_x-SP composite powders with SiO_x-SPs smaller than 500 nm exhibit both localized absorption peaks and diffuse absorption, whereas those with larger SiO_x-SPs exhibit localized absorption peaks only (Figure 2b versus Figure 2c; Figure 3a versus b). The diffuse absorption shows a linear dependence on the loading of Pt ufMNPs (Figure 3c, open circles and dashed line), indicating the uniform electric fields

of the diffuse light around individual SiO_x-SPs. In contrast, the localized absorption peaks show a superlinear dependence on the loading of Pt ufMNPs regardless of the size of SiO_x-SPs (Figure 3c,d, diamond symbols and solid lines), confirming that the scattering resonances generate enhanced electric fields with nonuniform distributions near the surface of individual SiO_x-SPs (see the example shown in Figure S2). With increased coverage of Pt ufMNPs on the SiOx-SPs, more local "hot spots" of enhanced electric fields near the SiO_x surface are occupied with the Pt ufMNPs to contribute to the overall optical absorption of the composite powders. The power exponent of the superlinear dependence increases with the size of SiO_x -SPs. For instance, the power exponent is 1.41 for the localized absorption peak (at 312 nm) of the composite powder with 262 nm SiO_x-SPs, and it increases to 1.62 for the averaged absorbance of all peaks of the sample with 1089 nm SiO..-SPs.

The scattering behavior of SiO_x-SPs in the composite powders is also influenced by the packing density of composite particles, thus affecting the optical absorption of the Pt-ufMNPs/SiO_x-NS composite powders (Figure 4). For example, when 2.5 wt % Pt ufMNPs are loaded on the SiO_x-SPs with a diameter of 262 nm and dried in an oven (Figure 4a), the powder exhibits absorption peaks originating from

both localized absorption (at 312 nm) and photonic-reflectionattenuated diffuse absorption (at 488 nm) and the uphill tail at longer wavelengths (Figure 4c, dotted curve). When an aqueous dispersion of the composite particles is freeze-dried, more and large voids are left in the dried sample with a much lower packing density (Figure 4b). The presence of a larger void volume does not change the number and positions of the absorption peaks determined by the localized scattering resonances of individual SiO_x-SPs and the photonic stop band of the self-assembled superlattices (Figure 4c, dashed curve). The large voids in the freeze-dried powder sample only reduce the sizes of individual domains of photonic superlattices, whereas the periodicity of the superlattices is still the same to maintain the photonic stop band. The reduced packing density lowers the diffuse absorbance but not the localized absorption, indicating that the larger voids generated from freeze-drying are mainly located within the powders rather than on the sample surface compared to the sample dried in an oven. On the other hand, compressing the powders dried in an oven to form pellets can squeeze out voids to increase the packing density and darken the appearance (Figure S14). Forming the condensed pellets increases both the localized absorption peaks and the diffuse absorption (Figure 4d). The exclusion of voids in the pellets restricts the diffusion of gas (or liquid) to access the Pt ufMNPs buried in the pellets, deteriorating their performance in applications such as photocatalysis.

The electric fields of the diffuse light interacting with the ufMNPs are usually weaker than the incident light, whereas the electric fields contributing to the localized absorption are much stronger than the incident light because of light scattering resonances near the SiO_x-SP's surfaces. Such differences in electric fields originating from different scattering mechanisms can influence the processes sensitive to electric fields. The absorbance of a sample is usually linearly dependent on the number of Pt ufMNPs that interact with and absorb light. When a Pt-ufMNPs/SiO_x-SP composite powder sample containing small SiO_x-SPs exhibits the same absorbance as a sample containing large SiO_x-SPs, more Pt ufMNPs are involved in the former sample to absorb the diffuse light, while fewer Pt ufMNPs are involved in the latter sample to absorb the locally enhanced light. Under this condition, the light-matter interactions in single Pt ufMNPs supported on differently sized SiO_x-SPs may behave differently. For example, hot-electron photocatalysis may exhibit a superlinear dependence of reaction kinetics on high illumination power density (or square of the electric field), 9,19,34,35 implying that, at high enough power density to generate superlinear dependence, the Pt-ufMNPs/SiO_x-SP composite particles with dominating localized absorption may favor hot-electron photocatalysis under intense illumination.

4. CONCLUSIONS

Optical absorption of ufMNPs dispersed on dielectric SiO_x -SPs of different sizes has been systematically studied with the absorption-sensitive DRS and theoretical calculations, revealing that the SiO_x -SPs in the composite powder samples exhibit three types of scattering to determine optical absorption of the ufMNPs in the UV–vis–NIR spectral range (i.e., 300-1100 nm). The localized scattering resonances near the surface of SiO_x -SPs support the observation of well-defined (sharp) peaks in the DRS spectra, and the number and position of the absorption peaks depend on the size of the SiO_x -SPs. The

intensity shows a superlinear dependence on the loading of ufMNPs, highlighting the nonuniform distribution of "hot spots", i.e., strong electric fields enhanced by the localized scattering resonances. The nonunidirectional diffuse scattering allows a portion of the light to penetrate the composite powder to be absorbed by the supported ufMNPs. The corresponding optical absorbance is linearly proportional to the loading of ufMNPs, indicating that electric fields of the diffuse light are uniform near the surface of individual ufMNPs. Diffuse light is dominant in the sample containing small SiO_x-SPs because of the primary contribution from Rayleigh scattering that exhibits strong wavelength dependence. Light of a longer wavelength penetrates deeper than the light of a shorter wavelength, resulting in a peakless uphill absorption profile as a function of wavelength. Such a wavelength-dependent uphill profile becomes less profound for the samples containing large SiO_x-SPs because scattering transits to less-wavelengthdependent Mie scattering with the increase of particle size. Moreover, the high dimensional uniformity of SiO_x-SPs makes a ufMNPs/SiO_x-SP composite sample to self-assemble into ordered superlattices (or small photonic crystals) to modulate the diffuse light, exhibiting a reflection peak at the stop band where the diffuse light is reduced to show a valley in the DRS spectrum of the composite powder. The appearance of the valley in the DRS spectrum results in an asymmetric and broad peak, which is different from the narrow and symmetric peaks originating from the localized scattering resonances. Differentiating the origins of different optical absorption peaks is important to understanding and rationally controlling the optical absorption of ufMNPs/SiO_x-SP composite powders, which will benefit the exploration of their applications requiring different electric fields. For example, the applications relying on the nonlinearity of electric fields could benefit from the composite particles with large SiO_x-SPs that are dominated by localized (enhanced) optical absorption.

ASSOCIATED CONTENT

Supporting Information

The Supporting Information is available free of charge at https://pubs.acs.org/doi/10.1021/acs.jpcc.2c04303.

Synthesis procedure of Pt ufMNPs on mesoporous silica nanoparticles; calculation of the absorption cross-section of freestanding Pt ufMNPs; calculation of photonic crystal stop bands; photosnapshot and diagram of setup configuration for DRS measurement; SEM and TEM images of Pt ufMNPs/SiO_x-SP composite particles; SEM images of assembled powder samples; SEM image of the pellet samples; near-field intensity maps and theoretical modeled spectra; absorption spectrum of Pt ufMNPs; DRS and scattering spectra of SiO_x-SPs; calculated absorption/scattering spectra of Pt ufMNPs and SiO_x-SPs; schematic diagram of the effective medium model for composite particles; peak comparison between calculated and measured scattering resonance peaks; comparison between calculated and measured photonic stop band positions; and assignment of peaks in the DRS spectra (PDF)

AUTHOR INFORMATION

Corresponding Author

Yugang Sun – Department of Chemistry, Temple University, Philadelphia, Pennsylvania 19122, United States;

o orcid.org/0000-0001-6351-6977; Email: ygsun@temple.edu

Authors

Qilin Wei — Department of Chemistry, Temple University, Philadelphia, Pennsylvania 19122, United States

Matas Simukaitis — Department of Chemistry, Temple
University, Philadelphia, Pennsylvania 19122, United States
Siyu Wu — Department of Chemistry, Temple University, Philadelphia, Pennsylvania 19122, United States;
orcid.org/0000-0002-0199-5471

Jonathan J. Foley, IV – Department of Chemistry, University of North Carolina Charlotte, Charlotte, North Carolina 28223, United States; orcid.org/0000-0001-8814-4444

Complete contact information is available at: https://pubs.acs.org/10.1021/acs.jpcc.2c04303

Author Contributions

The manuscript was written with the contributions of all authors. All authors have given approval to the final version of the manuscript. Q.W. and M.S. contributed equally.

Notes

The authors declare no competing financial interest.

ACKNOWLEDGMENTS

The work was supported by Temple University. Electron microscopy characterizations were performed using the facilities hosted in the Temple Materials Institute (TMI), Temple University. J.J.F., IV gratefully acknowledges financial support NSF CAREER Award (Grant No. CHE-2043215). Computational resources were provided, in part, by the MERCURY consortium (http://mercuryconsortium.org/) under the NSF (Grant Nos. CHE-1229354, CHE-1662030, and CHE-2018427).

REFERENCES

- (1) Ha, M.; Kim, J.-H.; You, M.; Li, Q.; Fan, C.; Nam, J.-M. Multicomponent Plasmonic Nanoparticles: From Heterostructured Nanoparticles to Colloidal Composite Nanostructures. *Chem. Rev.* **2019**, *119*, 12208–12278.
- (2) Jaque, D.; Martínez Maestro, L.; del Rosal, B.; Haro-Gonzalez, P.; Benayas, A.; Plaza, J. L.; Martín Rodríguez, E.; García Solé, J. Nanoparticles for Photothermal Therapies. *Nanoscale* **2014**, *6*, 9494–9530
- (3) Jain, P. K.; Huang, X.; El-Sayed, I. H.; El-Sayed, M. A. Noble Metals on the Nanoscale: Optical and Photothermal Properties and Some Applications in Imaging, Sensing, Biology, and Medicine. *Acc. Chem. Res.* **2008**, *41*, 1578–1586.
- (4) Luo, S.; Ren, X.; Lin, H.; Song, H.; Ye, J. Plasmonic Photothermal Catalysis for Solar-to-fuel Conversion: Current Status and Prospects. *Chem. Sci.* **2021**, *12*, 5701–5719.
- (5) Baffou, G.; Bordacchini, I.; Baldi, A.; Quidant, R. Simple Experimental Procedures to Distinguish Photothermal from Hotcarrier Processes in Plasmonics. *Light: Sci. Appl.* **2020**, *9*, 108.
- (6) Richardson, H. H.; Carlson, M. T.; Tandler, P. J.; Hernandez, P.; Govorov, A. O. Experimental and Theoretical Studies of Light-to-heat Conversion and Collective Heating Effects in Metal Nanoparticle Solutions. *Nano Lett.* **2009**, *9*, 1139–1146.
- (7) Brongersma, M. L.; Halas, N. J.; Nordlander, P. Plasmon-induced Hot Carrier Science and Technology. *Nat. Nanotechnol.* **2015**, *10*, 25–34.
- (8) Cortés, E.; Grzeschik, R.; Maier, S. A.; Schlücker, S. Experimental Characterization Techniques for Plasmon-assisted Chemistry. *Nat. Rev. Chem.* **2022**, *6*, 259–274.

- (9) Linic, S.; Aslam, U.; Boerigter, C.; Morabito, M. Photochemical Transformations on Plasmonic Metal Nanoparticles. *Nat. Mater.* **2015**, *14*, 567–576.
- (10) Zhan, C.; Wang, Q.-X.; Yi, J.; Chen, L.; Wu, D.-Y.; Wang, Y.; Xie, Z.-X.; Moskovits, M.; Tian, Z.-Q. Plasmonic Nanoreactors Regulating Selective Oxidation by Energetic Electrons and Nanoconfined Thermal Fields. *Sci. Adv.* **2021**, *7*, No. eabf0962.
- (11) Wang, C.; Astruc, D. Nanogold Plasmonic Photocatalysis for Organic Synthesis and Clean Energy Conversion. *Chem. Soc. Rev.* **2014**, *43*, 7188–7216.
- (12) Hartland, G. V.; Besteiro, L. V.; Johns, P.; Govorov, A. O. What's So Hot about Electrons in Metal Nanoparticles? *ACS Energy Lett.* **2017**, *2*, 1641–1653.
- (13) Stewart, S.; Wei, Q.; Sun, Y. Surface Chemistry of Quantum-sized Metal Nanoparticles Under Light Illumination. *Chem. Sci.* **2021**, 12, 1227–1239.
- (14) Zhu, X. Y. Electron Transfer at Molecule-metal Interfaces: A Two-photon Photoemission Study. *Annu. Rev. Phys. Chem.* **2002**, *53*, 221–247.
- (15) Hägglund, C.; Zeltzer, G.; Ruiz, R.; Thomann, I.; Lee, H.-B.-R.; Brongersma, M. L.; Bent, S. F. Self-assembly Based Plasmonic Arrays Tuned by Atomic Layer Deposition for Extreme Visible Light Absorption. *Nano Lett.* **2013**, *13*, 3352–3357.
- (16) Harutyunyan, H.; Martinson, A. B. F.; Rosenmann, D.; Khorashad, L. K.; Besteiro, L. V.; Govorov, A. O.; Wiederrecht, G. P. Anomalous Ultrafast Dynamics of Hot Plasmonic Electrons in Nanostructures with Hot Spots. *Nat. Nanotechnol.* **2015**, *10*, 770–774.
- (17) Dongare, P. D.; Zhao, Y.; Renard, D.; Yang, J.; Neumann, O.; Metz, J.; Yuan, L.; Alabastri, A.; Nordlander, P.; Halas, N. J. A 3D Plasmonic Antenna-reactor for Nanoscale Thermal Hotspots and Gradients. *ACS Nano* **2021**, *15*, 8761–8769.
- (18) Li, K.; Hogan, N. J.; Kale, M. J.; Halas, N. J.; Nordlander, P.; Christopher, P. Balancing Near-field Enhancement, Absorption, and Scattering for Effective Antenna—reactor Plasmonic Photocatalysis. *Nano Lett.* **2017**, *17*, 3710—3717.
- (19) Swearer, D. F.; Zhao, H.; Zhou, L.; Zhang, C.; Robatjazi, H.; Martirez, J. M. P.; Krauter, C. M.; Yazdi, S.; McClain, M. J.; Ringe, E.; Carter, E. A.; Nordlander, P.; Halas, N. J. Heterometallic Antennareactor Complexes for Photocatalysis. *Proc. Natl. Acad. Sci. U. S. A.* **2016**, *113*, 8916–8920.
- (20) Naiki, H.; Uedao, T.; Wang, L.; Tamai, N.; Masuo, S. Multiphoton Emission Enhancement from a Single Colloidal Quantum Dot Using SiO₂-Coated Silver Nanoparticles. *ACS Omega* **2017**, 2, 728–737.
- (21) Feng, A. L.; You, M. L.; Tian, L.; Singamaneni, S.; Liu, M.; Duan, Z.; Lu, T. J.; Xu, F.; Lin, M. Distance-dependent Plasmonenhanced Fluorescence of Upconversion Nanoparticles using Polyelectrolyte Multilayers as Tunable Spacers. Sci. Rep. 2015, S, 7779.
- (22) Ausman, L. K.; Schatz, G. C. Whispering-gallery Mode Resonators: Surface Enhanced Raman Scattering without Plasmons. *J. Chem. Phys.* **2008**, *129*, No. 054704.
- (23) Codrington, J.; Eldabagh, N.; Fernando, K.; Foley, J. J., IV Unique Hot Carrier Distributions from Scattering-mediated Absorption. *ACS Photonics* **2017**, *4*, 552–559.
- (24) Liu, N.; Shi, L.; Zhu, S.; Xu, X.; Yuan, S.; Zhang, X. Whispering Gallery Modes in a Single Silica Microparticle Attached to an Optical Microfiber and Their Application for Highly Sensitive Displacement Sensing. *Opt. Express* **2018**, *26*, 195–203.
- (25) Price, M. B.; Lewellen, K.; Hardy, J.; Lockwood, S. M.; Zemke-Smith, C.; Wagner, I.; Gao, M.; Grand, J.; Chen, K.; Hodgkiss, J. M.; et al. Whispering-gallery Mode Lasing in Perovskite Nanocrystals Chemically Bound to Silicon Dioxide Microspheres. *J. Phys. Chem. Lett.* 2020, 11, 7009–7014.
- (26) Zhang, N.; Han, C.; Xu, Y.-J.; Foley, J. J., IV; Zhang, D.; Codrington, J.; Gray, S. K.; Sun, Y. Near-field Dielectric Scattering Promotes Optical Absorption by Platinum Nanoparticles. *Nat. Photonics* **2016**, *10*, 473–482.

- (27) Rasamani, K. D.; Sun, Y. Promoting Reactivity of Photoexcited Hot Electrons in Small-Sized Plasmonic Metal Nanoparticles that are Supported on Dielectric Nanospheres. *J. Chem. Phys.* **2020**, *152*, No. 084706.
- (28) Dai, X.; Rasamani, K. D.; Wu, S.; Sun, Y. Enabling Selective Aerobic Oxidation of Alcohols to Aldehydes by Hot Electrons in Quantum-sized Rh Nanocubes. *Mater. Today Energy* **2018**, *10*, 15–22.
- (29) Dai, X.; Rasamani, K. D.; Hall, G.; Makrypodi, R.; Sun, Y. Geometric Symmetry of Dielectric Antenna Influencing Light Absorption in Quantum-sized Metal Nanocrystals: A Comparative Study. Front. Chem. 2018, 6, 494.
- (30) Wei, Q.; Guzman, K. G.; Dai, X.; Attanayake, N. H.; Strongin, D. R.; Sun, Y. Highly Dispersed RuOOH Nanoparticles on Silica Spheres: An Efficient Photothermal Catalyst for Selective Aerobic Oxidation of Benzyl Alcohol. *Nano-Micro Lett.* **2020**, *12*, 41.
- (31) Rasamani, K. D.; Foley, J. J., IV; Beidelman, B.; Sun, Y. Enhanced Optical Absorption in Semiconductor Nanoparticles Enabled by Nearfield Dielectric Scattering. *Nano Res.* **2017**, *10*, 1292–1301.
- (32) Rayleigh, L. On the Electromagnetic Theory of Light. *Philos. Mag.* **1881**, *12*, 81–101.
- (33) Mie, G. Beiträge Zur Optik Trüber Medien, Speziell Kolloidaler Metallösungen. *Ann. Phys.* **1908**, *330*, *377*–445.
- (34) Busch, D. G.; Ho, W. Direct Observation of the Crossover from Single to Multiple Excitations in Femtosecond Surface Photochemistry. *Phys. Rev. Lett.* **1996**, *77*, 1338–1341.
- (35) Ho, W. Reactions at Metal Surfaces Induced by Femtosecond Lasers, Tunneling Electrons, and Heating. J. Phys. Chem. 1996, 100, 13050–13060.

☐ Recommended by ACS

Engineering Optical Absorption in Late Transition-Metal Nanoparticles by Alloying

Christopher Tiburski and Christoph Langhammer

DECEMBER 13, 2022 ACS PHOTONICS

READ 🗹

Quantitatively Revealing the Anomalous Enhancement in Shell-Isolated Nanoparticle-Enhanced Raman Spectroscopy Using Single-Nanoparticle Spectroscopy

Shu Hu, Jian-Feng Li, et al.

DECEMBER 05, 2022

ACS NANO

READ 🗹

Photochemistry of Ethanol on Rutile TiO₂(110): Breaking Two Bonds with One Hole

Yuemiao Lai, Qing Guo, et al.

JANUARY 18, 2023

THE JOURNAL OF PHYSICAL CHEMISTRY C

RFAD **「**✓

Universal Theory of Light Scattering of Randomly Oriented Particles: A Fluctuational-Electrodynamics Approach for Light Transport Modeling in Disordered Nanostructures

Francisco V. Ramirez-Cuevas, Ioannnis Papakonstantinou, et al.

FEBRUARY 04, 2022

ACS PHOTONICS

READ 🗹

Get More Suggestions >